Current Science International
Volume: 11 | Issue: 04| Oct. – Dec.| 2022

EISSN:2706-7920 ISSN: 2077-4435
DOI: 10.36632/csi/2022.11.4.31
Journal homepage: www.curresweb.com
Pages: 402-417

Impact of Recent Advances in Implant Surface Structure on Stress Distribution in Different Directions of Load Application: A Finite Element Analysis

Wessam M. Dehis[1] and Sherif Aly Sadek [2]

[1]Associate Professor at Fixed and Removable Prosthodontics Department, Oral and Dental Research Institute, National Research Centre, Cairo, Egypt.
[2]Associate Professor at Prosthodontic Department, Faculty of Dentistry, Cairo University, Cairo, Egypt.

Received: 11 Oct. 2022 **Accepted:** 10 Nov. 2022 **Published:** 20 Nov. 2022

ABSTRACT

Edentulism is a co-morbidity to numerous systemic and oral defects as; diabetes, osteoporosis and alveolar bone deficiency frequently challenge the dental implant therapy success. Implant's design and surface alterations have a considerable impact on the magnitude and pattern of stresses distributed sequential to the massive occlusal forces and bite strokes applied to dental implants avoiding major bone defects and consequent implant's failure. This study aimed to both assess and compare the impact of two dissimilar implant surface structures on stress distribution in maxillary implant supported removable partial overdenture (RPOD) utilizing three-dimensional (3D) Finite element analysis (FEA). Results: The present study revealed that Implant B (Trabecular Metal Zimmer implants) values were much less than those of Implant A (Straumann Roxolid SLActive implants) regarding stress distribution for maxillary implant supported RPOD. Conclusion: The trabecular porous tantalum implant can provide better distribution of stress among cortical and cancellous bone and can be a promising substitute for providing successful implant survival rate. Further research and clinical studies are recommended regarding porous tantalum implants with different prosthetic appliances especially the maxillofacial obturators and compromised cases as osteoporosis patients.

Keywords: Implant surface structure, Stress distribution, Load Application, Finite Element Analysis, Implant supported removable partial overdenture

1. Introduction

Edentulism and remarkable teeth loss are chief difficulties frequently occurring globally and exceedingly especially in the developing world. Tremendous biological alternations usually take place post teeth loss. Such changes include impaired masticatory efficiency, alveolar bone remodeling, transformed microflora composition, altered taste sensation, poor esthetics and psychological complications. Thus, edentulism is a co-morbidity to numerous systemic and oral defects as, diabetes, osteoporosis and alveolar bone deficiency (Felton 2009; Hiraki *et al.,* 2008; Sompop *et al.,* 2014).

Dental implant performs a reliable remedy format for the prosthodontic therapy of both partially and completely edentulous patients. Hence, enhancing function and aesthetics, but both systemic and oral co-morbidities of edentulism frequently challenge the dental implant therapy success. Plentiful clinical strategies have evolved to accomplish implant treatment successfully as, proactively limiting the bone volume loss after to tooth extraction, bone augmentation by guided bone regeneration, grafts, membranes and employing short narrow implants as well (Sompop *et al.,* 2014; El Chaar *et al.,* 2019; Kelly *et al.,* 2019).

Although molar and premolar regions are critical zones for implant positioning than the anterior one, since the posterior bone area is characterized for having diminished density, limited vertical volume and superior occlusal forces. The implant's long term survival rate in implant supported overdentures is multifactorial. Not only relies on age, sex, type of bone and splinting of implants, but also depends on

Corresponding Author: Wessam M. Dehis, Agric. Eng. Res. Inst., Agric. Res. Center, Dokki, Giza, Egypt.
E-mail: wewedehis@gmail.com

implant's number, distribution, design, fabrication process, material and surface treatment (Edgard and Alejandro 2017; De-Liz *et al.,* 2016; Boven *et al.,* 2015).

Nowadays, the dental implant's key material is the biologically "inert"; Titanium (Ti). However, the advantageous criteria of commercially pure Ti grade 4 promoted its utilization in dental implant construction, yet lately it has been proved that additional modifications to the Ti implant's material and surface criteria have a prime impact in monitoring the cell response and enhance implant's success rate. Titanium implants exceed cell proliferation, accelerate bone formation around fixture and diminish bone strains (Brigitte *et al.,* 2015; Hotchkiss *et al.,* 2016; Pinar *et al.,* 2016).

The Titanium implant's surface crucially influences the osteointegration process via alteration of the material's chemical and wettability criteria which convert the cell's response towards the implanted material. Accordingly, diverse surface adjustments have been applied employing both additive and subtractive procedures including surface topography and chemistry modulation, acid etching, surface coatings, anodization and sand blasting to achieve crestal bone maintenance as well as osseointegration acceleration and strengthening (Pellegrini *et al.,* 2018; Rupp *et al.,* 2018; Helena *et al.,* 2021).

It has been previously hypothesized that premature failure of machined surface implants is subsequent to surface roughness deficiency. Clinical considerations proved that the machined implant's surface area is directly proportional to its rough surface, which gradually improves cell attachment, enhance osteogenesis and boost implant stability which enables immediate and early loading protocol (Wennerberg *et al.,* 2018; Peter *et al.,* 2019).

Implant surface structure modification by establishing rough surface has been approached by construction of pores. This takes place through sintering titanium beads onto titanium alloy providing micropores ranging from to 400 μm in size with ~35% porosity. Hence, Porous tantalum (Ta)-based, trabecular-structured biomaterial with ~80% porosity is an exact module of porous biomaterials industrialized to improve implant fixation by covering a vitreous carbon scaffold with elemental Ta via a chemical vapor deposition (CVD) procedure. Hence, porous tantalum metal augments the bone implant contact and helps the success of dental implant therapy in certain populations (Kelly *et al.,* 2019; David *et al.,* 2020; Ayshin *et al.,* 2021).

Accordingly, implant's design and surface alterations have a considerable impact on the magnitude and pattern of stresses distributed sequential to the massive occlusal forces and bite strokes applied to dental implants ending up with major bone defects and consequent implant's failure. Such stresses can simply be visualized through the object's internal micro movements successive to any versatile forces, calculating and analyzing process known as the finite element analysis (FEA). (Ayshin *et al.,* 2021; Mathur *et al.,* 2011; Yushan *et al.,* 2022).

Therefore, evaluation of these forces' magnitude, distribution and impact on both bone height and density is crucial.

2. Materials and Methods

This study aimed to both assess and compare the impact of two dissimilar implant surface structures [Straumann Roxolid SLActive implants *(Roxolid_ SLActive_ (Institute Straumann AG, Basel Switzerland)* and Trabecular Metal Zimmer implants *(Trabecular Metal™ Dental Implant, Zimmer Biomet, Palm Beach Gardens, FL, USA)* on stress distribution in maxillary implant supported RPOD utilizing three-dimensional (3D) Finite Element Analysis (FEA).

A three-dimensional (3D) mesh model of a partially edentulous maxilla free from any craniofacial abnormalities was applied by employing Mimics *(Materialise®, Belgium)*, accompanied by reconstruction, conversion and exportation of a 3D voxel model as stereo-lithographic format of Sound Transmission Loss (STL) files. These STL files were imported into Exocad *(EXOCAD ®, 2008, Germany)* for further smoothening and exported as STL format (Fig.1a). Based on further contemplates, abutments of each implant system have been utilized as a Telescopic attachment. Such abutments together with Heat cure acrylic resin removable partial overdenture were performed utilizing the Exocad (Fig.1b) then superimposed on the maxilla's model. (Gregory and Oliver 2009; Oliver *et al.,* 2006) (Fig.1c).

Accordingly, models were imported to Geomagic Design X software for renovating them into solid parts and creating implant with abutment as a Telescopic attachment. Then superimposition of implants, abutments (attachments), both cortical and cancellous bones, gingiva and RPOD portions

EISSN: 2706-7920 ISSN: 2077-4435 **DOI: 10.36632/csi/2022.11.4.31**

together took place for Boolean subtraction to attain the maxilla's 3D Computer aided design (CAD) model (Fig.1d).

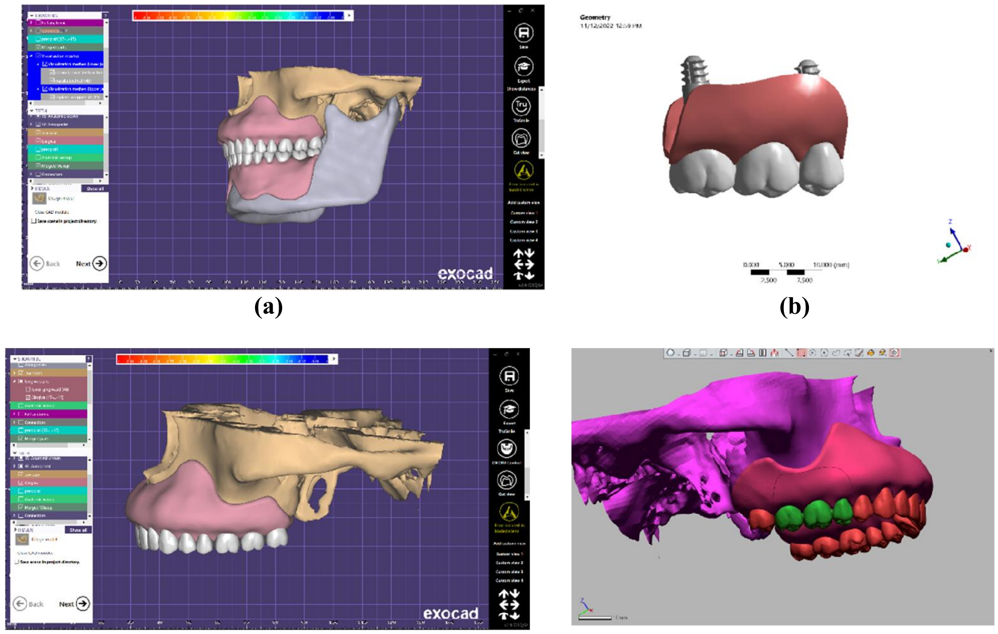

(a) **(b)**

(c) **(d)**

Fig. 1: a: The maxilla's model imported to Exocad for smoothening **b:** The implant supported RPOD was created utilizing Exocad **c:** The implant supported RPOD was superimposed on the maxilla using Exocad **d:** Reverse engineering of the maxilla into Geomagic Design X software.

Regarding the Implant supported removable partial overdenture, two geometric models were designed; one for two Straumann Roxolid SLActive implants, abutments employed as Telescopic attachments *(Roxolid SLActive (Institute Straumann AG, Basel Switzerland)* type (A) implant supported RPOD, the other for two Trabecular Metal Zimmer implants, abutments acting as Telescopic attachments *(Trabecular Metal™ Dental Implant, Zimmer Biomet, Palm Beach Gardens, FL, USA)* type (B) implant supported RPOD based on these two-implant systems user manual using identical size for utilized implants (Fig. 2 a&b).

(a) **(b)**

Fig. 2: a: Design of the Straumann Roxolid SLActive implant with abutment (Telescopic attachment). **b:** Design of the Trabecular Metal Zimmer implant with abutment (Telescopic attachment) using Geomagic Design X software.

The model's construction ultimate phase was assembling the components, where all the solid parts were both imported and gathered. Thereafter, superimposition of the implant, abutment (attachment), premolar and the RPOD fragments synchronously were accomplished with both cortical and sponge bone for Boolean subtraction to attain the 3D CAD model of the maxilla and were lastly exported as Parasolid extension files (Fig. 3).

Curr. Sci. Int., 11(4): 402-417, 2022
EISSN: 2706-7920 ISSN: 2077-4435 **DOI: 10.36632/csi/2022.11.4.31**

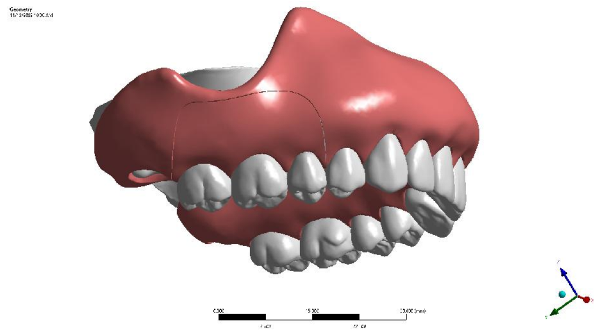

Fig. 3: 3D CAD model of the assembled maxilla as Parasolid extension file.

Concerning the stress linear static analysis, there are two crucial parameters that should be defined; elastic (Young's) modulus and Poisson's Ratio, which simply define the stress strain curve's linear part of any isotropic material. Values of the material criteria were defined and assumptions were made based on the previously published studies and manufacturer's data. All the model components; implant, abutment (attachment), screw, RPOD, cortical and spongy bone were considered for being isotropic, homogenous and linearly elastic materials. Young's modulus of elasticity and Poisson's Ratio of all materials employed in this contemplate were listed in Table (1).

Table 1: Physical properties of each component of the model.

Material	Modulus of Elasticity	Poisson's Ratio
Compact Bone	13700 MPa	0.3
Cancellous Bone	7930 MPa	0.3
Heat Cure Acrylic Resin Denture Base	2770 MPa	0.35
Titanium Alloy	110000 MPa	0.33

Two models were generated comprising these two sorts of implants utilized, together with distribution of each type unilaterally to be subjected to forces applied in vertical, bucco-palatal, palato-buccal and disto-mesial directions.

During meshing, each model was divided into small parts named elements connected together at points termed nodes forming an unstructured mesh (Fig. 4). The total number of elements and nodes in each model is blotted in Table (2).

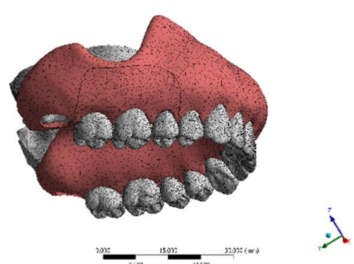

Fig. 4: Meshed model of the assembled maxilla.

Table 2: The total number of elements and nodes in each model.

Model	Number of Elements	Number of Nodes
Model Implant Type A	7385410	11833678
Model Implant Type B	1254400	19451693

Analyzing the stress state required applying four techniques of loads with a common value of 250 N, (Vertically / a bucco-palatal load with 20 degree inclination / a palato-buccal load with 20 degree inclination/ a disto-mesial load with 20 degree inclination) were induced on the central fossa of the premolar and molar bilaterally utilizing 3D finite element ball model (5.8 mm in diameter) to the premolar and molar's occlusal surface at a three loading points; two points on the inner slopes of both the mesio-buccal and disto-buccal cusps and a one point on the inner slope of the mesio-palatal one (Fig. 5 a, b, c & d).

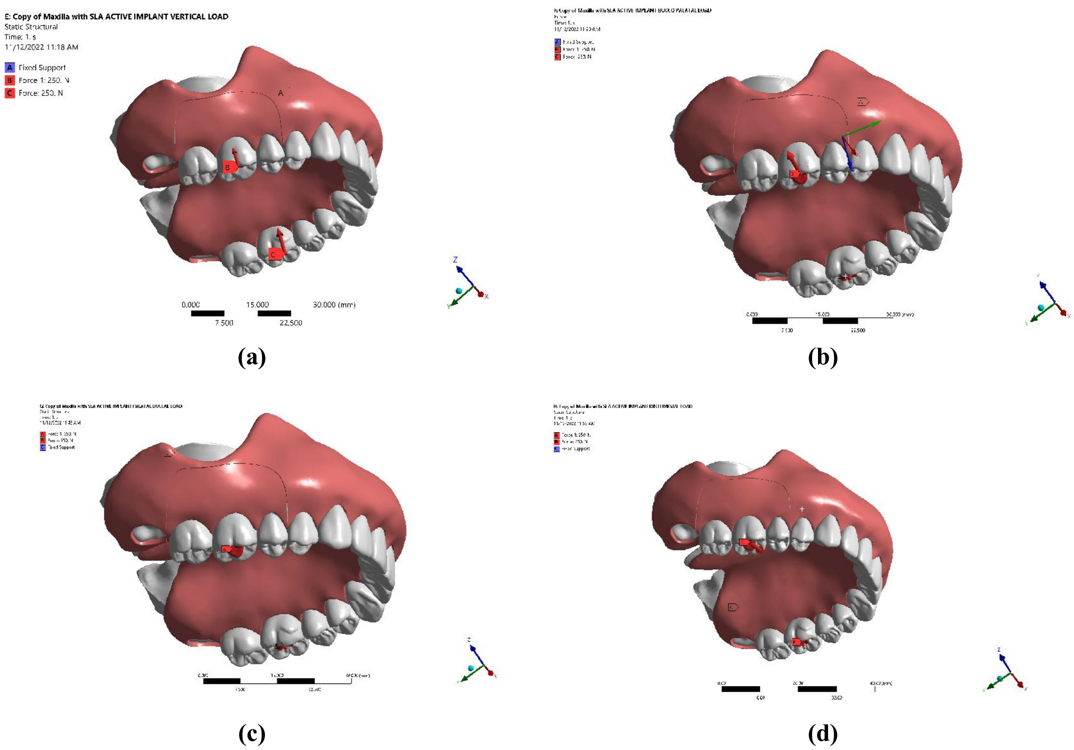

Fig. 5: Applying load of 250 N bilateral on the molar central fossa for both models Implant Type A and B. **a:** Vertical. **b:** Palato-buccal. **c:** Bucco-palatal. **d:** Disto-mesial.

Subsequent to creating the 3D meshes and determining the loads, a boundary condition was demarcated that all movements at the maxilla's base were restrained through load application in all directions. Hence, a boundary condition (zero displacement) was applied at the bottom nodes of the maxilla in directions (X, Y and Z) (Fig. 6).

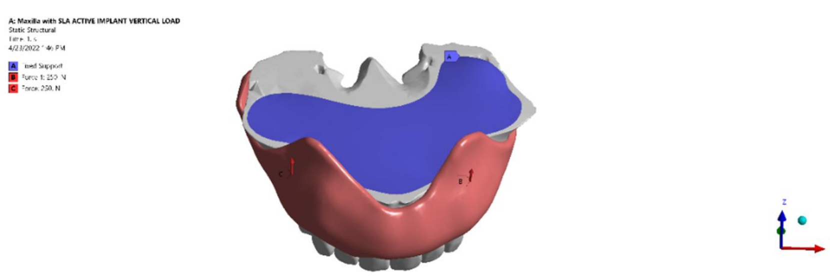

Fig. 6: Zero displacement support applying.

Every model was analyzed with the same exact boundary conditions and load application. The stresses induced in the maxilla during the load application were calculated and recorded to be analyzed.

3. Results

Analysis of the study models was performed regarding two major parameters; stress (Maximum principal and Von-Misses stress) and displacement.

3.1. Maximum Principal Stress

Assessment of stresses in the maxilla took place at the implant to bone contact in the premolar and molar region. The stress figure was indicated as a colored bar drawn on the right side of each figure and stress values were designated in Mega Pascal (MPa). The colors' spectrum illustrating (Max. principal stress) in a descending order was red, orange, yellow, light green, turquoise, light blue and dark blue. Thus, areas with red color signified the highest stress values while those with dark blue one characterized the lowermost stress standards. The supreme principal stress values in every zone were verified for each model on four planes. The virtual bone-surrounding tooth and implant models were alienated into 3 regions to simplify stress pattern analysis.

3.2. SEqv: Von-Misses Stress

The stresses were standardized on the implant occlusally. The stress figure was marked as a colored bar drawn on the right side of each figure and the stress values were indicated in Mega Pascal (MPa). The extreme equivalent Von-Misses stress values in every zone were documented for every model on four planes. The simulated implant models were alienated into 3 regions to simplify analysis of the stress pattern which are coronal, body and apex.

3.3. Maximum Principal Stress Values Induced on The Implant to Bone Contacts:

Table (3), Figures (7-10) and Charts (1&2) signify the extreme quantity of Maximum principal stresses induced around the implant to bone contact. The results of this study revealed that the implant presence have a huge influence on the stress concentration in the maxilla, on the molar and premolar side. Maximal principal stress of both implant classes utilized in both regions was mainly concentrated coronally, apart from that the molar region implants when subjected to distomesial force, more stresses were apically concentrated.

a) Maximal principal stress in premolar region:

- Implant A displayed extra stress concentration coronally when load was vertically directed and least with the distomesial route.
- Implant B demonstrated additional stress concentration coronally when load was distomesially directed and least with the vertical path.

b) Maximal principal stress in molar region:

- Generally, the maximum concentration of stress for both implants took place coronally in all directions of load applied, except only with the distomesial application of force, as the stress was excessively more apically concentrated even from the coronal reading with other pathways of load.

Table 3: Maximum principal stress induced on bone at the implant to bone contact in two models.

Maximum Principal Stress on Premolar									
	Implant A					Implant B			
	Vertical	Bucco-palatal	Palato-buccal	Disto-mesial		Vertical	Bucco-palatal	Palato-buccal	Disto-mesial
Coronal	4.20	1.41	3.32	1.30	**Coronal**	0.53	0.78	0.99	1.12
Body	0.08	0.03	0.10	0.12	**Body**	0.05	0.04	0.08	0.03
Apex	0.14	0.10	0.25	0.20	**Apex**	0.12	0.11	0.22	0.25
Maximum Principal Stress on Molar									
	Implant A					Implant B			
	Vertical	Bucco-palatal	Palato-buccal	Disto-mesial		Vertical	Bucco-palatal	Palato-buccal	Disto-mesial
Coronal	3.75	0.91	1.94	2.80	**Coronal**	0.95	1.38	0.67	0.37
Body	0.02	0.03	0.02	0.40	**Body**	0.00	0.12	0.12	0.05
Apex	1.38	0.65	0.23	4.50	**Apex**	0.18	0.21	0.28	3.22

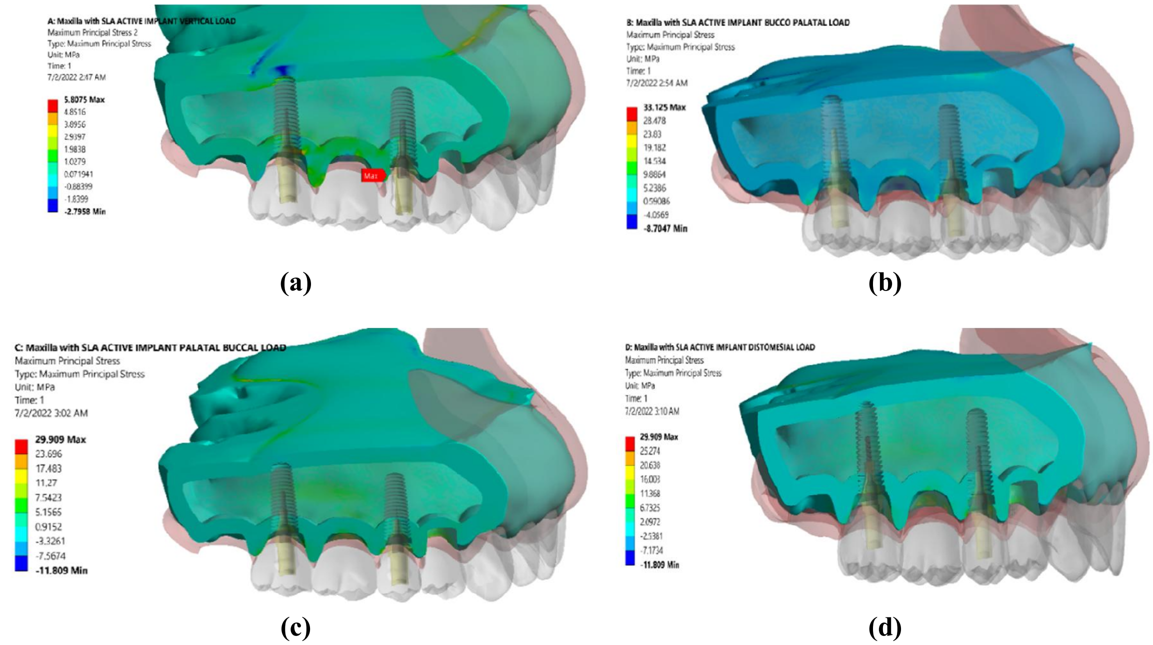

Fig. 7: Maximum principal stress distribution applying 250 N load on compact bone model implant A. **a:** Vertical. **b:** Bucco-palatal. **c:** Palato-buccal. **d:** Disto mesial.

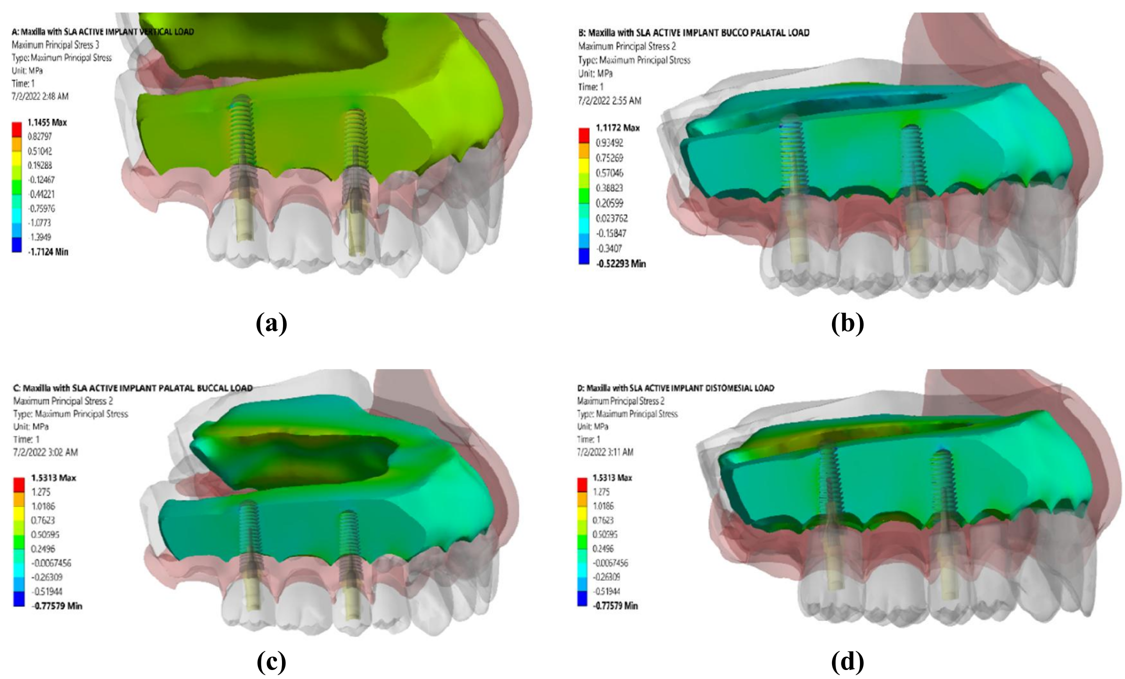

Fig. 8: Maximum principal stress distribution applying 250 N load on cancellous bone model implant A. **a:** Vertical. **b:** Bucco-palatal. **c:** Palato-buccal. **d:** Disto mesial.

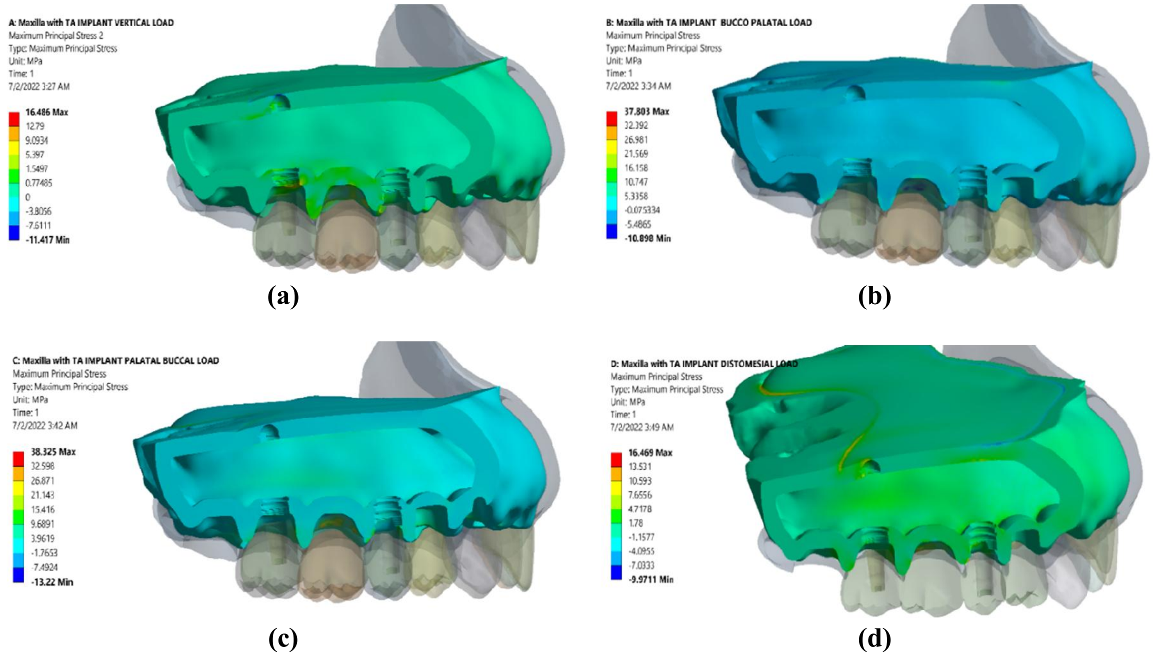

Fig. 9: Maximum principal stress distribution applying 250 N load on compact bone model implant B. **a:** Vertical. **b:** Bucco-palatal. **c:** Palato-buccal. **d:** Disto mesial.

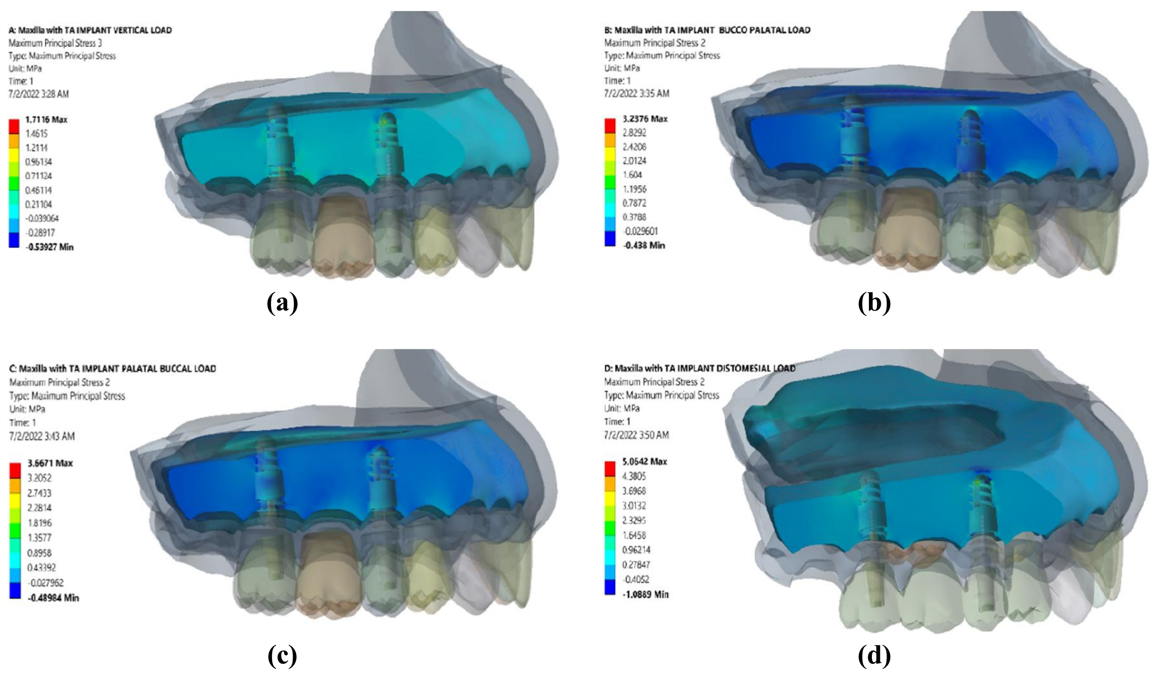

Fig. 10: Maximum principal stress distribution applying 250 N load on cancellous bone model implant B. **a:** Vertical. **b:** Bucco-palatal. **c:** Palato-buccal. **d:** Disto mesial.

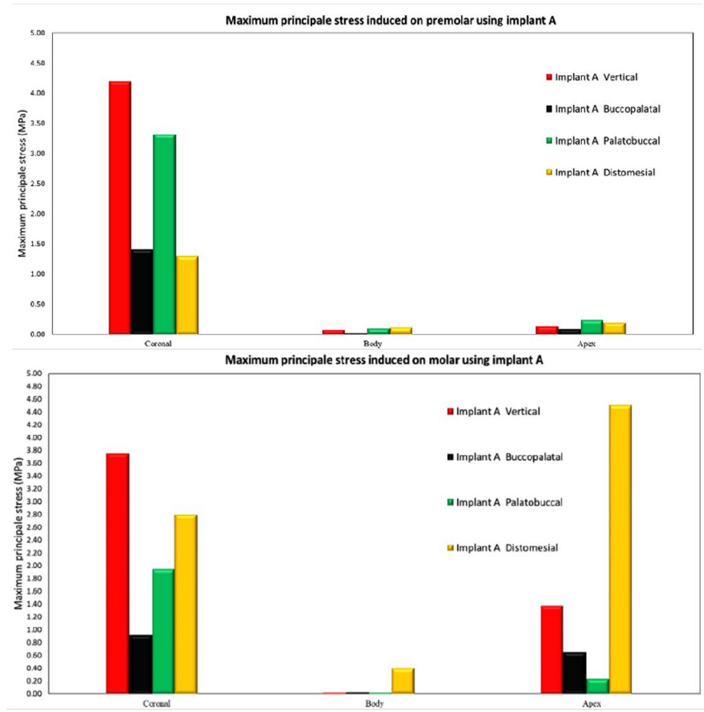

Chart 1: Maximum principal stress distribution on model (A) molar and first premolar.

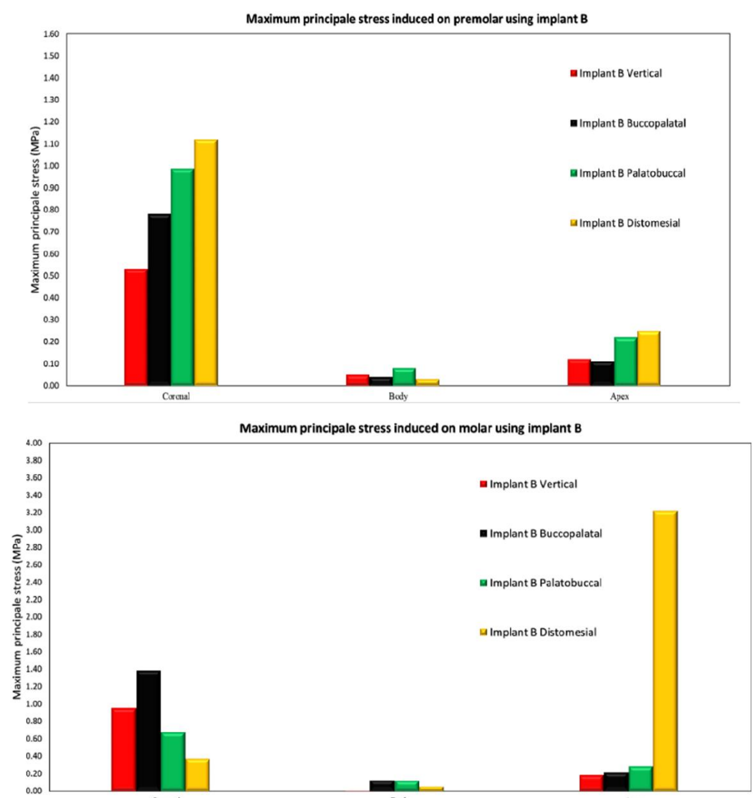

Chart 2: Maximum principal stress distribution on model (B) molar and first premolar.

c) Von-Misses Stress Values Induced on The Implant to Abutment Contacts:

Table (4), Figures (11-12) and Charts (3&4) represent the utmost standards of Von-Misses stresses induced around the implant to bone and abutment contacts. This consideration's results revealed the huge impact of the load angulation on the stress concentration on the molar and premolar side of the maxilla.

d) Von-Misses stress values induced on implant to abutment contact:

- Implant A, implant to abutment region has the highest stress concentration in both premolar and molar regions, at the coronal region and declined gradually towards the apical area.
- Implant B, the highest stress concentration in both premolar and molar regions took place in that sequence; apically, coronally and then the mid-region.

e) Von- Misses stress on premolar implant:

- Implant A illustrated further stress concentration coronally with the bucco-palatal application of load and least with the distomesial one.
- Implant B displayed extra stress concentration apically with the palato-buccal application of load, as it concentrates first coronally then apically and terminates at the mid- part.

f) Von-Misses stress on molar implant:

- Implant A revealed extra stress concentration coronally when load was applied palato-buccally and least with vertically applied load, except when load was vertically applied the stress concentration was more apically.
- Implant B displayed further stress apically when force was applied vertically and least with the distomesial application of load except with the bucco-palatal direction of load where stress was concentrated more coronally.

Table 4: Von-Misses stress induced implant to abutment contact in two models.

Von-Misses Stress on Premolar Implant									
	Implant A					**Implant B**			
	Vertical	**Bucco-palatal**	**Palato-buccal**	**Disto-mesial**		**Vertical**	**Bucco-palatal**	**Palato-buccal**	**Disto-mesial**
Coronal	10.80	22.34	8.19	6.23	**Coronal**	0.85	4.39	9.85	4.68
Body	1.68	4.68	2.32	1.45	**Body**	0.77	1.12	3.25	6.80
Apex	1.23	0.85	1.31	2.20	**Apex**	4.89	5.86	6.52	10.68
Von-Misses Stress on Molar Implant									
	Implant A					**Implant B**			
	Vertical	**Bucco-palatal**	**Palato-buccal**	**Disto-mesial**		**Vertical**	**Bucco-palatal**	**Palato-buccal**	**Disto-mesial**
Coronal	18.26	97.31	105.88	104.20	**Coronal**	6.38	12.83	7.35	6.35
Body	12.26	1.47	3.20	3.23	**Body**	3.86	3.65	3.80	2.70
Apex	67.49	7.83	8.65	9.55	**Apex**	22.34	8.68	9.80	8.65

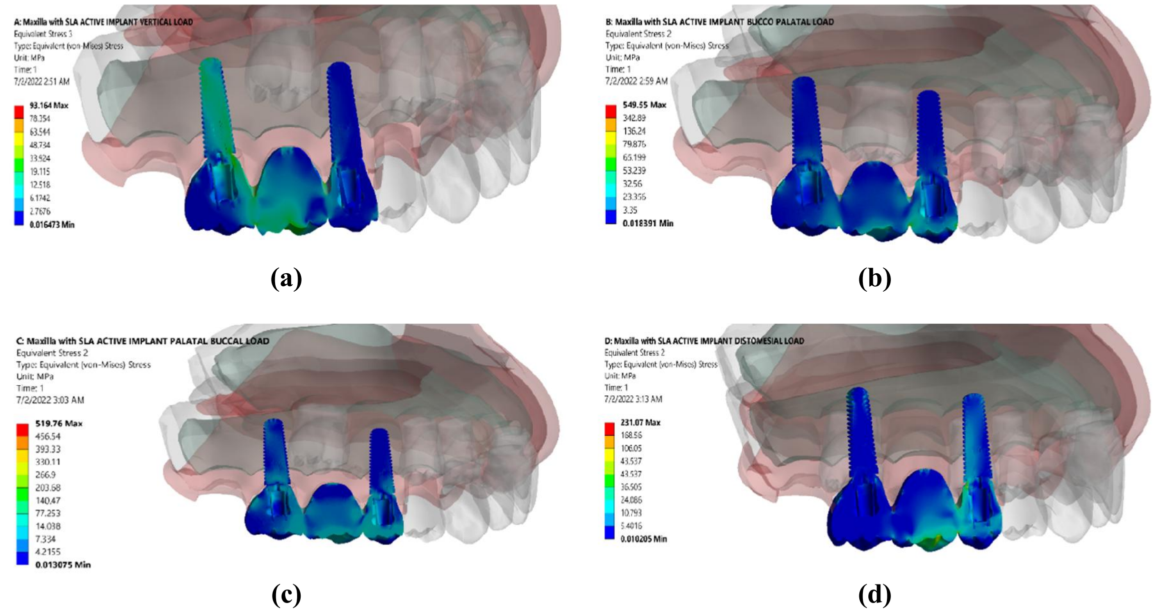

Fig. 11: Von-Misses stress distribution applying load of 250 N load occlusally to implant A.
a: Vertical. **b:** Bucco-palatal. **c**: Palato-buccal. **d**: Disto mesial.

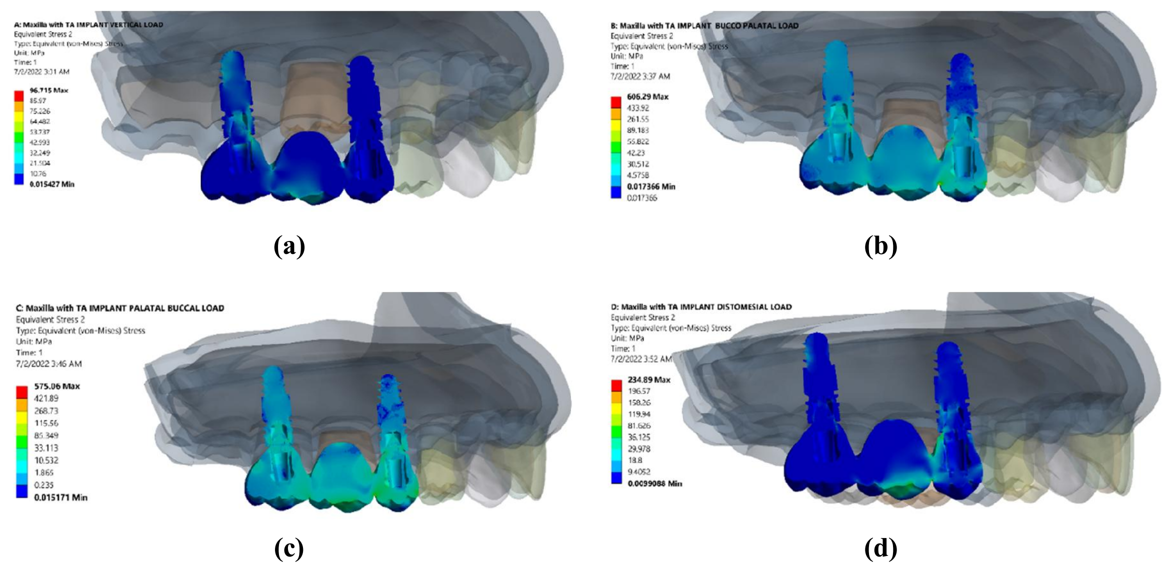

Fig. 12: Von-Misses stress distribution applying load of 250 N load occlusally to implant B.
a: Vertical. **b:** Bucco-palatal. **c:** Palato-buccal. **d:** Disto mesial.

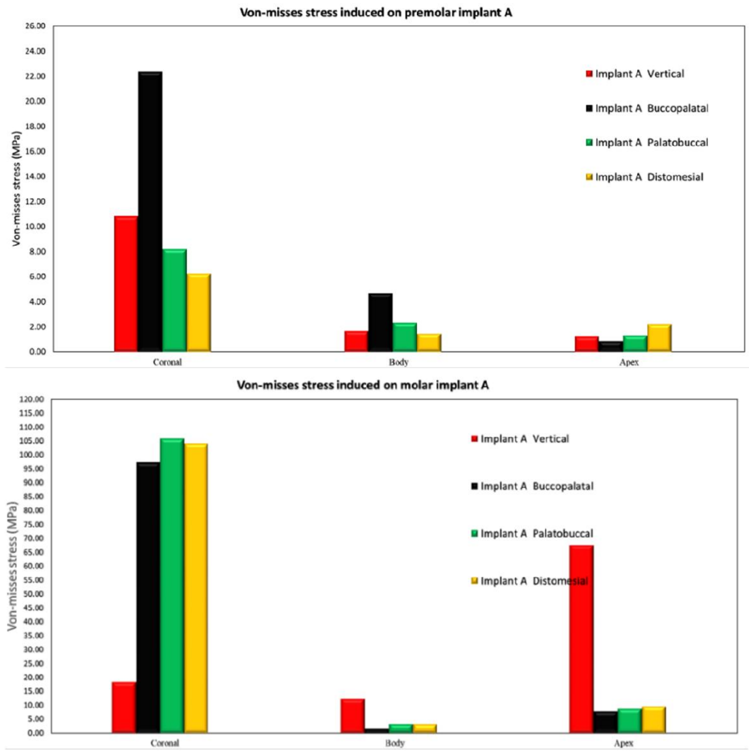

Chart 3: Von-Misses stress distribution on model A implant at molar and first premolar sides.

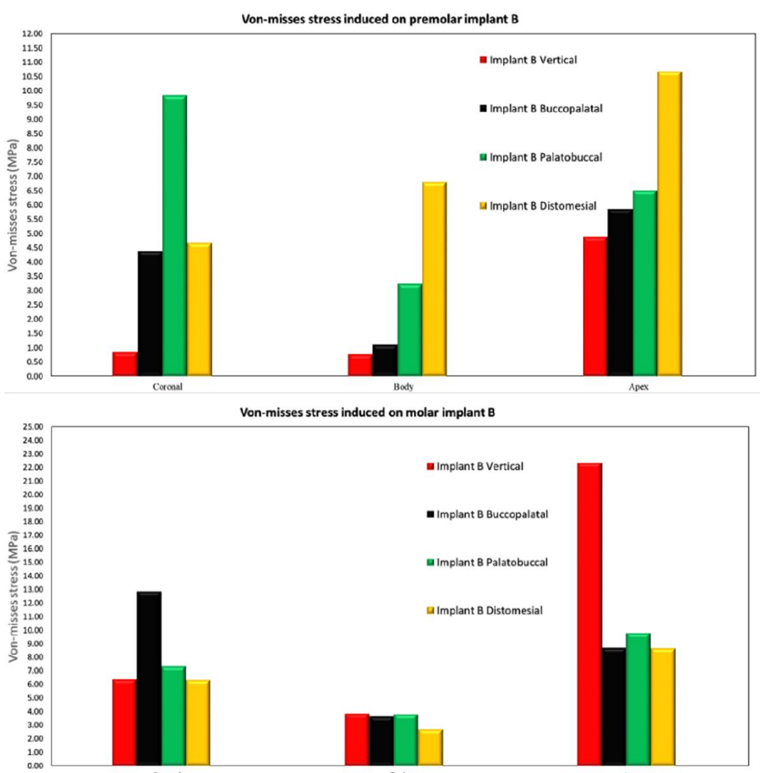

Chart 4: Von-Misses stress distribution on model B implant at molar and first premolar sides.

As a whole, the present contemplate's results revealed that implant B (Trabecular Metal Zimmer implants) values were much less than those of Implant A (Straumann Roxolid SLActive implants) regarding stress distribution.

4. Discussion

Dental implant offers the best consistent handling modality for versatile forms of edentulism and persistently provides an efficacious intervention in a broad diversity of clinical scenarios. Hence, it is considered as the utmost heavily load bearing fixture that can withstand extensive forces and huge stresses applied on it in dissimilar routes (Chrcanovic *et al.,* 2017; David *et al.,* 2019)**.**

Although, there are diverse factors and conditions that compromise the fixture's prognosis, yet the implant's surface structure performs a crucial role in osseointegration and thus drives tremendous research surveys on the impact of surface structure alterations on osteogenic potentiality (Peter *et al.,* 2019; Smeets *et al.,* 2016).

Abutments of each implant system have been utilized as a Telescopic attachment in implant supported RPOD to provide additive means of retention and stability besides their non resilient rigid nature which distributes the actual forces without absorbing or altering them, hence promotes sending all stresses applied on the implant and facilitates assessment of load applied in different direction (Gregory and Oliver 2009; Oliver *et al.,* 2006).

The maxillary implant supported removable partial overdenture of both Implant types (A) and (B) employed in this study were placed in the premolar and molar region since it habitually reveals to some extent implant's inferior survival rates than the anterior ones. This might be attributed to such maladies as uncontrolled diabetes, osteoporosis or periodontitis, as well as tooth extraction, maxillary sinus pneumatization and prolonged utilization of conventional tissue-supported prosthesis. Sequentially, remarkable deficiency in alveolar bone dimensions, inferior density and inadequacy of vertical volume of bone posteriorly, together with the extensive occlusal forces take place. Furthermore, though numerous grafting methods and distraction osteogenesis have made draft fruitful fluctuations in posterior jaw augmentation, yet bone of minimal density characteristically originates in these areas may prevail post grafting. Thus, implant survival rate in augmented posterior jaw is currently debatable (Edgard and Alejandro 2017; Sheridan *et al.,* 2016; Misawa *et al.,* 2016).

Outcomes of the Maximal principal stress values at premolar region biologically revealed that extra strain values took place coronally at the cortical bone surrounding both; implant A with vertical route of forces and Implant B on applying distomesial force direction. On the other hand, once the distomesial route of forces were applied at Implant A and vertical ones at Implant B, the least stress concentration values appeared coronally beneath the biological resistance limits of bone. Regarding the molar zone implants A and B, their Maximal principal stress values with diverse directions of forces applied were mostly concentrated coronally in the compact bone region. While, such stress values diminished gradually and were more apically concentrated on applying distomesial force at the two types of molar region implants.

This is attributed to the variant modulus of elasticity in both cortical and spongy bones. The advanced modulus of elasticity in cortical bone is extra resistant to deformation and bears further load than the cancellous one. Furthermore, it has been reported that trabecular metal (B) implant diminishes the strain around both cortical and trabecular bone especially with vertically applied forces at molar region and enhance prolonged survival rate of implant supported RPOD by diminishing the marginal loss of bone (Ayshin *et al.,* 2021; Chang *et al.,* 2016).

Speaking about Von-Misses stress, although the stress values around both implant and abutment were insignificant yet this indicates for the degree of implant's stability according to its type. In Implant A, implant to abutment (attachment) section has the uppermost stress concentration in both premolar and molar regions coronally and declined progressively towards the apical area, this is due to the Cantilever's angle and impact resulted from load applied. While in Implant B, the highest stress concentration in both premolar and molar areas took place at the apical region followed by coronal one (implant to abutment region) then the mid area.

Such outcomes are simply explained by the distinctive nature between cortical and cancellous bone segments together with the Tantalum porous (B) implants concerning their modulus of elasticity and degree of distortion resistance. This is further confirmed by other studies which attempted that porous tantalum implants (B) are extra advantageous in contrast to the standard Titanium (Ti) ones (A).

Modulus of elasticity is a good illustration; as the elastic modulus of porous tantalum in Gigapascals was (1.3–10 GPa) is considerably identical to that of both cortical (12–18 GPa) and cancellous bone (0.1–0.5 GPa), compared to that of the most common materials Titanium and Ti alloy implants (106–115 GPa). Thus, porous tantalum (B) fixtures diminish the impact of stress which aids in preserving peri-implant bone density and enhance implants success (Kelly *et al.,* 2019; Ayshin *et al.,* 2021; Chang *et al.,* 2016).

Moreover, results of this study revealed that the greatest Von-Misses stress on the cortical segments of bone were broadly advanced than those at cancellous ones assessing the maximum stresses applied on implant A. Thus, excessive forces are directed towards the crestal bone, which accordingly destruct the cortical one and increase its resorption. On the contrary was Von-Misses stress of implant B which were extreme at cancellous bone segments than at the cortical ones. This was attributed to the maximum concentration of stresses apically than coronally. Thus, excessive forces are directed away from the crestal bone, which sequentially preserve the cortical one and minimize its resorption (Ayshin *et al.,* 2021; Topkaya and Solmaz 2015; Chang *et al.,* 2016).

As a sequala, it is hypothesized employing the porous tantalum trabecular implant (B) as a helpful choice for less dense bone patients. This is allocated to application of moderately rough surface implants habitually osseointegrate faster, remarkably diminish early failures, aid in areas with minimal density of bone and permit application of immediate loading protocols. As manufacturing of porous surface structure is one of the tremendous implant surface modification approaches which aimed to enhance osseointegration (David *et al.,* 2020; Ayshin *et al.,* 2021).

Moreover, it has been claimed that porous structure of tantalum implants not only grant bone-implant contact with enlarged surface area but also both permit and facilitate revascularization to promote formation, development and preservation of new bone via permitting the speedy growth and proliferation of endothelial cells through the trabecular implant structure. Thus, biomechanical stability of tantalum fixture is established successive to the newly formed bone; on the implant surface as well as within the initial bone-implant gap through the implant's both peripheral and deep pores. This terminates with remodeling of the existing bone that primarily anchored the implant, promoting the porous tantalum implant by time to be homogenously attached to bone (David *et al.,* 2020; Ayshin *et al.,* 2021).

5. Conclusion and Recommendations

Within the limitations of the present study, it has been concluded that:

1- Implant's surface structure is the utmost chief parameter manipulating massive concentration and distribution of stress in both maxillary molar and premolar areas.
2- The trabecular porous tantalum implant (B) can provide better distribution of stress among cortical and cancellous bone and can be a promising substitute for providing successful implant survival rate.

Further research and clinical studies are recommended regarding porous tantalum implants with different prosthetic appliances especially the maxillofacial obturators and compromised cases as osteoporosis patients.

List of Abbreviations

RPOD: Removable Partial Overdenture
3D: Three-dimensional
FEA: Finite Element Analysis
STL: Sound Transmission Loss
N: Newton
Ti: Titanium
GPa: Gigapascals
CVD: Chemical Vapor Deposition
Ta: Tantalum
CAD: Computer Aided Design
CAM: Computer Aided Manufacturing
SEqv: Von-Misses Stress
MPa: Mega Pascal
CBCT: Cone Beam Computed Tomography

Declarations

- **Ethics Approval and Consent to Participate: "**Not applicable"
- **Consent for Publication: "**Not applicable"
- **Availability of Data and Materials: "**The datasets used and/or analyzed during the current study are available from the corresponding author on reasonable request."
- **Competing Interests: "**The authors declare that they have no competing interests"
- **Funding: "**The authors declare that this research is self-funded."

References

Ayshin, A., H. Yasser, and S. Fariba, 2021. Evaluation of stress distribution of porous tantalum and solid titanium implant-assisted overdenture in the mandible: A finite element study. Dental Research Journal, 18:108.

Boven, G., G. Raghoebar, A. Vissink, and H. Meijer, 2015. Improving masticatory performance, bite force, nutritional state and patient's satisfaction with implant overdentures: A systematic review of the literature. J. Oral Rehabil., 42:220-33.

Brigitte, S., R. Sylvie, B. Simon, D. Nicholas, and M. Katharina, 2015. The role of nanostructures and hydrophilicity in osseointegration: In-vitro protein-adsorption and blood-interaction studies. J. Biomed. Mater Res., 103:2661-2672.

Chang, S., S. Huang, S. Huang, and C. Lin, 2016. Mechanical response comparison in an implant overdenture retained by ball attachments on conventional regular and mini dental implants: A finite element analysis. Comput Methods Biomech. Biomed. Engin., 19:911-21.

Chrcanovic, B., T. Albrektsson, and A. Wennerberg, 2017. Bone quality and quantity and dental implant failure: A systematic review and meta-analysis. International Journal of Prosthodontics, 30(3):219-237.

David, F., F. Paul, E. Carlo, and M. Luiz, 2020. Biomechanical analysis of the osseointegration of porous tantalum implants. J. Prosthet Dent., 123(6):811-820.

David, F., M. Gustavo, S. Elisa, F. Paul, E. Carlo, and M. Luiz, 2019. Bone response to porous tantalum implants in a gap-healing model. Clin. Oral I., 30:156-168.

De-Liz, P., F. Da Fontoura, E. Rivaldo, P. Mattia, R. Vidal, and E. Fernandes, 2016. Satisfaction level and masticatory capacity in edentulous patients with conventional dentures and implant-retained overdentures. Braz. J. Oral Sci., 5:1232-8.

Edgard, E., and C. Alejandro, 2017. A Retrospective Survival Study of Trabecular Tantalum Implants Immediately Placed in Posterior Extraction Sockets Using a Flapless Technique. Journal of Oral Implantology, 43(2): 115-124.

El Chaar, E., Z. Lei, Z. Yongsheng, R. Sandgren, J. Fricain, M. Dard, B. Pippenger, and S. Catros, 2019. Osseointegration of Superhydrophilic Implants Placed in Defect Grafted Bones. International Journal of Oral & Maxillofacial Implants, 34(2): 443-450.

Felton, D., 2009. Edentulism and comorbid factors. J. Prosthodont, 18(2):88-96.

Gregory, G., and H. Oliver, 2009. Year study of implant placement in regenerated bone and rehabilitation with telescopic crown retained dentures: A case report. Journal of Oral Implantology, 35(6):303-309.

Helena, F., F. Gary, B. Fabien, S. Rebecca, H. Valentin, W. Nils, and E. Benjamin, 2021. Peri-implant bone preservation of a novel, self-cutting, and fully tapered implant in the healed crestal ridge of minipigs: submerged vs. transgingival healing. Clinical Oral Investigations, 25:6821-6832.

Hiraki, A., K. Matsuo, T. Suzuki, T. Kawase, and K. Tajima, 2008. Teeth loss and risk of cancer at 14 common sites in Japanese. Cancer Epidemiol Biomarkers Prev., 17(5):1222-1227.

Hotchkiss, K., G. Reddy, S. Hyzy, Z. Schwartz, B. Boyan, and N. Olivares, 2016. Titanium surface characteristics including topography and wettability, alter macrophage activation. Acta Biomater, 31:425-34.

Kelly, M., T. Kegan, and O. Rene, 2019. Novel in vitro comparative model of osteogenic and inflammatory cell response to dental implants. Journal of Dental Materials, 35:176-184.

Mathur, A., V. Pai, S. Nandini, and A. Sarmah, 2011. Finite element analysis of dental implant as orthodontic anchorage. The Journal of Contemporary Dental Practice, 12(4): 259-264.

Misawa, M., J. Lindhe, and M. Arau´jo, 2016. The alveolar process following single-tooth extraction: a study of maxillary incisor and premolar sites in man. Clin. Oral Implants Res., 27:884-889.

Oliver, H., B. Christian, N. Dimitris, and G. Gregory, 2006. Telescopic crowns as attachments for implant supported restorations: A case series. Journal of Oral Implantology, 32(6):291-299.

Pellegrini, G., L. Francetti, B. Barbaro, and M. Del Fabbro, 2018. Novel surfaces and osseointegration in implant dentistry. J. Investig. Clinc. Dent., 9(4): 12349.

Peter, S., G. Roland, and B. Sebastian, 2019. Al_2O_3 Particles on Titanium Dental Implant Systems following Sandblasting and Acid-Etching Process. Hindawy International Journal of Biomaterials, 5:1-11.

Pinar, A., C. Gulsen, G. Onur, O. Caner, and E. Hakan, 2016. Stability and Marginal Bone Level Changes of SLActive Titanium-Zirconium Implants Placed with Flapless Surgery: A Prospective Pilot Study. Clinical Implant Dentistry and Related Research, 18(6):1193-1199.

Rupp, F., L. Liang, J. Geis-Gerstorfer, L. Scheideler, and F. Hüttig, 2018. Surface characteristics of dental implants. Dent. Mater, 34:40-57.

Sheridan, R., A. Decker, A. Plonka, and H. Wang, 2016. The role of occlusion in implant therapy: A comprehensive updated review. Implant Dent., 25:1-10.

Smeets, R., B. Stadlinger, and F. Schwarz, 2016. Impact of dental implant surface modifications on osseointegration. BioMed Research International, 1: 1-16.

Sompop, B., C. Warren, A. Sandra, H. Bashir, L. Austin, R. Glenn, M. Thiago, and O. Steven, 2014. Development and Applications of Porous Tantalum Trabecular Metal Enhanced Titanium Dental Implants. Clin. Implant Dent. Relat. Res., 16(6): 817-826.

Topkaya, T., and M. Solmaz, 2015. The effect of implant number and position on the stress behavior of mandibular implant retained overdentures: A three-dimensional finite element analysis. J. Biomech., 48:2102-9.

Wennerberg, A., T. Albrektsson, and B. Chrcanovic, 2018. Long-term clinical outcome of implants with different surface modifications. European Journal of Oral Implantology, 11(1): 123-136.

Yushan, Y., J. Jiuyang, F. Song, H. Jieying, W. Yamei, Y. Qinghe, W. Wei, L. Jinsong, and C. Shaohai, 2022. Optimization Analysis of Two-Factor Continuous Variable between Thread Depth and Pitch of Micro-implant under Toque Force. Hindawi Computational and Mathematical Methods in Medicine, 1:1-10.